

## Influence of Hall current and Joule heating on entropy generation during electrokinetically induced thermoradiative transport of nanofluids in a porous microchannel\*

B. MALLICK, J. C. MISRA<sup>†</sup>, A. R. CHOWDHURY

Centre for Healthcare Science and Technology, Indian Institute of Engineering Science  
and Technology, Shibpur, Howrah 711103, India

(Received Jan. 26, 2019 / Revised May 24, 2019)

**Abstract** A comprehensive theoretical study of entropy generation during electrokinetically driven transport of a nanofluid is of prime concern in the paper. The flow is considered to take place on a wavy channel under the action of an external transverse magnetic field and an external pressure gradient. Navier slips at the walls of the channel and thermal radiation have been taken into account in the study. The theoretical study has been carried out by developing a mathematical model by taking into account the effects of Joule heating, viscous dissipation, and the transverse magnetic field on heat transfer during the electrokinetic transport of the fluid. The derived analytical expressions have been computed numerically by considering the nanofluid as a mixture of blood and ferromagnetic nanoparticles. Variations in velocity, streaming potential, temperature distribution, Nusselt number, and Bejan number associated with the electrokinetic flow in capillaries have been investigated by the parametric variation method. The results have been presented graphically. The present investigation reveals that streaming potential decreases due to the Hall effect, while for the cooling capacity of the microsystem, we find an opposite behavior due to the Hall effect. The study further reveals that the fluidic temperature is reduced due to increase in the Hall current, and thereby thermal irreversibility of the system is reduced significantly. The results presented here can be considered as the approximate estimates of blood flow dynamics in capillaries during chemotherapy in cancer treatment.

**Key words** electrokinetic induction, Hall current, nanofluid, porous media, thermal transport, entropy generation

**Chinese Library Classification** O361

**2010 Mathematics Subject Classification** 34K10, 76D05, 76W05, 76S05, 76Z05, 80A20

\* Citation: MALLICK, B., MISRA, J. C., and CHOWDHURY, A. R. Influence of Hall current and Joule heating on entropy generation during electrokinetically induced thermoradiative transport of nanofluids in a porous microchannel. *Applied Mathematics and Mechanics (English Edition)*, 40(10), 1509–1530 (2019) <https://doi.org/10.1007/s10483-019-2528-7>

<sup>†</sup> Corresponding author, E-mail: misrajc@gmail.com

Project supported by Science and Engineering Research Board (SERB), Department of Science and Technology, Government of India, New Delhi (No. CRG/2018/000153)

©Shanghai University and Springer-Verlag GmbH Germany, part of Springer Nature 2019

## 1 Introduction

Owing to their wide range of applications in physiology and medicine, studies on a variety of problems in microfluids and nanofluidics have been receiving growing attention of researchers in current years. Moreover, various technological processes and applications, including separation and analysis of chemical and biological samples, micro-electro-mechanical systems (MEMS), and material processing<sup>[1–3]</sup> have relevance to these newly emerging areas of research. Flows in microfluidic/nanofluidic devices are greatly affected by electrokinetic/electromagneto-hydrodynamics (EMHD) effects<sup>[4–6]</sup>. Various investigations related to electrokinetic flows in microfluidic devices have been performed by previous authors<sup>[7–15]</sup>. In these reports, it has been emphasized that in the electrokinetic/electroosmotic flows, owing to the interaction between an ionized solution and static charges on dielectric surfaces there occurs a thin layer of electrical charges. This layer is electrical charges, which is termed as the electrical double layer (EDL). The EDL consists of two regions, the stern layer and the diffuse layer. Because of the principle of electroneutrality, the liquid takes on an opposite charge in the EDL. In the presence of an external electrical field, the ions of the diffuse layer are set in motion. Thus, the fluid mass moves as a whole. This type of movement is the so-called electroosmotic flow (EOF). Studies on this type of flow are useful in many problems of real life, in industries as well as in physiology and medicine. Some of the studies made in the past have already been mentioned above. Among the recent publications, mention may be made of the studies reported by Jian<sup>[16]</sup>, Sinha and Shit<sup>[17]</sup>, and Zhao et al.<sup>[18–19]</sup>. References to some other publications in this area can be found in these papers<sup>[9–15]</sup>.

In the present study, the flow is considered to take place by an external pressure gradient in an environment, where ionic species are stimulated by the induced magnetic field in the direction of the pressure gradient. Owing to this, an electric current is generated. This is termed as the streaming current, and the corresponding potential difference is termed as streaming potential. This results in a movement of the ionic species in the direction opposite to that of flow driven by pressure. This movement gives rise to the so-called conduction current. In contrast to the case of flow driven by pressure, an electrical drag force is generated in the EDL.

Studies on deformation, flow, and heat transfer of blood and its constituents, such as plasma, erythrocytes, platelet, and white cells come under the purview of hemorheology (also sometimes termed as blood rheology). Magneto-hemorheology deals with only those problems that concern the rheological behavior of any constituent of blood when the blood vessels are subject to magnetic fields<sup>[20]</sup>. In medical tests like magnetic resonance angiography (MRA) and the magnetic resonance imaging (MRI), human body has to be exposed to strong magnetic environment. This is why magneto-hemorheology has occupied a central place in biomedical research today. Schenck<sup>[21]</sup> mentioned that during tests, human body can be safely exposed to magnetic fields of intensity 8 T. For sub-human primates, the safety limit is 16 T. Zhao et al.<sup>[18]</sup> studied the effect of a transverse magnetic field on the streaming potential and heat transfer during flow of a nanofluid in a microchannel. Although they considered the intensity of the magnetic field to be large, they did not account for the Hall current. However, as pointed out by Cowling<sup>[22]</sup>, for magnetic fields of large strength, the generalized Ohm's law should be modified to include Hall current. Zhao et al.<sup>[19]</sup> also presented a theoretical analysis for the heat transfer problem of a nanofluid flowing on a parallel plate microchannel, when the flow takes place due to the combined influence of streaming potential and pressure gradient, in the absence of any external magnetic field. Sinha and Shit<sup>[17]</sup> analyzed the problem of fully developed EMHD flow of blood through a capillary in presence of thermal radiation. In this study, although the applied magnetic field was considered to be sufficiently strong, the effect of Hall current was not taken into account.

In most of the investigations, referred to above, we notice that the effect of Hall current has been ignored, while applying Ohm's law in the respective analyses. However, when the system is

subject to a considerably strong magnetic field, many complex phenomena, such as Hall current and Joule heating occur in the electrically conducting flow region. Owing to these factors, the flow outline of the ionized liquid is likely to be changed significantly. It may be mentioned here that the occurrence of Hall current is largely due to the extra potential variation between the opposite sides of the conductor. The Hall effect is propagated inside the liquid mass by means of electrons, whereby the current density and the Lorentz force are significantly changed.

It may be mentioned further that the fluid motion is likely to experience an irreversible effect owing to heat transfer and viscous dissipation. In the realm of thermal engineering, the thermodynamic concept of entropy generation can be used to minimize entropy generation. This was suggested by Bejan<sup>[23]</sup> in solving the thermal convection problems. This approach was used by Singh et al.<sup>[24]</sup> in their study of flow of a nanofluid on microchannels. In another study, entropy generation was studied by Mahmoudi et al.<sup>[25]</sup> in the case of convection flow of a nanofluid in a magnetic environment. The authors made an observation that entropy generation is reduced due to the presence of nanoparticles and that the magnetic field bears the potential of augmenting the entropy generation. Matin and Khan<sup>[26]</sup> performed an entropy generation in their study of mass and heat transfer, for a situation when the fluid flow takes place electrokinetically under the action of an external pressure.

In view of all the above, it has been our endeavor in this communication to report the results of a study of entropy generation that we have carried out during the flow and heat transfer of a nanofluid on a channel having wavy geometry. The study pertains to a situation, when the flow is executed by the action of electrokinetic forces and an external pressure gradient under the action of a sufficiently strong magnetic field applied externally. In order to incorporate the effect of Hall current in the theoretical analysis, we have considered the modified form of the generalized Ohm's law that takes care of the Hall effect. In order to make the model applicable to microvascular flows in the circulatory system, we have taken into account porosity effect, viscous dissipation, and also the velocity slip at the wall. Effects of Joule heating and thermal radiation are accounted for. One distinctive merit of this study is that under the purview of a single mathematical model, we have incorporated multiple factors of hemorheological study in order to explore the role played by streaming potential, entropy generation, and heat transfer process on the electrokinetic flow behavior of the fluid. With an aim to exhibit the application, computational work has been carried out by considering the nanofluid as a mixture of blood and ferromagnetic nanoparticles. Thus, the results presented here for different physical variables can be considered as approximate estimates of the variables during chemotherapy used in cancer treatment.

## 2 The model and its analysis

We consider the EMHD flow behavior of a incompressible viscous electrically conducting nanofluid of effective dielectric constant  $\epsilon_{nf}$ . The fluid mass is supposed to move in a channel under the resultant action of a pressure-gradient ( $P_\xi = -\frac{dp^*}{d\xi^*}$ ) and an electric field  $E$  of strength  $E_\xi$ , under the influence of a transverse magnetic field  $B$  of strength  $B_0$ . The pressure gradient combined with the body forces is supposed to drive fluid from its initial steady-state condition. The walls of the channel are supposed to be made of the same material. Therefore, we consider that the zeta potential at the walls are equal. An EDL is formed in the neighborhood of the walls caused by interaction between the electrically charged walls and the nanoparticles of the fluid. The channel walls are supposed to have wavy geometry (see Fig. 1) which can be described mathematically as

$$H^*(\xi^*) = d^* - a^* \cos^2(\pi \xi^*/L), \quad (1)$$

in which  $a^*$  and  $L$  denote the amplitude and characteristic length of the channel, respectively, while  $d^*$  denotes the constant height of the channel. It is assumed that the height of the channel

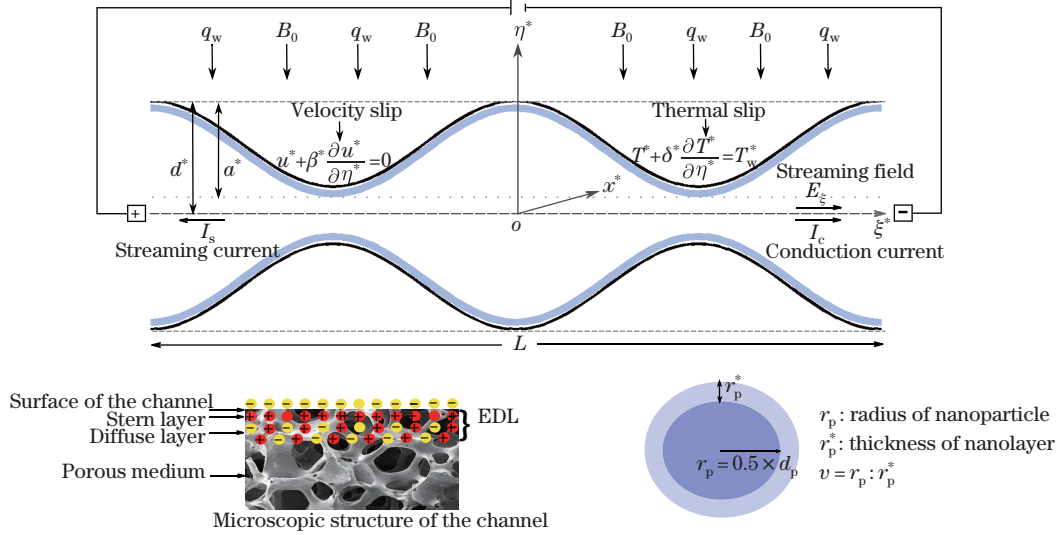


**Fig. 1** Physical configuration of the problem

is much less than its width and length ( $2H^* \ll W \ll L$ ).

Thermophysical properties of the nanofluid are supposed to be constants whose values are shown in Table 1. A constant heat flux  $q_w$  is imposed on the channel walls. As per requirement of the lab-on-a-chip (LOC) applications, this imposed heat flux  $q_w$  is considered to be positive.

**Table 1** Thermophysical properties of base fluid and nanoparticle<sup>[27–28]</sup>

Physical property	$\rho/$ ( $\text{kg}\cdot\text{m}^{-3}$ )	$c_p/$ ( $\text{J}\cdot\text{kg}^{-1}\cdot\text{K}^{-1}$ )	$k/$ ( $\text{W}\cdot\text{m}^{-1}\cdot\text{K}^{-1}$ )	$\sigma/$ ( $\text{S}\cdot\text{m}^{-1}$ )	$\epsilon/$ ( $\text{F}\cdot\text{m}^{-1}$ )
Base fluid (blood)	$1.08 \times 10^3$	$3.5 \times 10^3$	0.59	0.6	$2.03 \times 10^{-7}$
Nanoparticle ( $\text{Fe}_3\text{O}_4$ )	$5.2 \times 10^{-3}$	670	6	$2.5 \times 10^4$	80

## 2.1 Basic equations

Governing equations describing the steady transport mechanism of the nanofluids in a porous channel are given by

$$\nabla \cdot u = 0, \quad (2)$$

$$\rho_{\text{nf}}(u \cdot \nabla)u = -\nabla p^* + \nabla \cdot \tau - \frac{\mu_{\text{nf}}}{k^*}u + F_B, \quad (3)$$

$$(\rho c_p)_{\text{nf}}u \cdot \nabla T = k_{\text{nf}}\nabla^2 T - \nabla \cdot q + \frac{1}{\sigma_{\text{nf}}}J \cdot J + \tau \cdot \nabla u, \quad (4)$$

where  $\tau = \mu_{\text{nf}}(\nabla u + \nabla u^T)$  is the stress vector,  $u$  is the velocity vector, and  $\nabla p^*$  is the imposed pressure gradient,  $k^*$  is the permeability of the porous channel,  $T$  is the temperature,  $q$  is the radiative heat flux,  $J$  is the current density, while  $\rho_{\text{nf}}$  stands for the effective density of the nanofluid,  $\mu_{\text{nf}}$  is the effective viscosity of nanofluid,  $(\rho c_p)_{\text{nf}}$  is the effective heat capacitance,  $k_{\text{nf}}$  is the effective thermal conductivity of nanofluid, and  $\sigma_{\text{nf}}$  is the effective electrical conductivity of the nanofluid, which can be measured by using the following equations<sup>[29–30]</sup>:

$$\begin{cases} \rho_{\text{nf}} = \phi \rho_s + (1 - \phi) \rho_f, & \mu_{\text{nf}} = \mu_f / (1 - \phi)^{2.5}, & (\rho c_p)_{\text{nf}} = \phi (\rho c_p)_s + (1 - \phi) (\rho c_p)_f, \\ \frac{\sigma_{\text{nf}}}{\sigma_f} = 1 + \frac{3(\sigma_s - \sigma_f)\phi}{(\sigma_s + 2\sigma_f) - (\sigma_s - \sigma_f)\phi}, & \frac{k_{\text{nf}}}{k_f} = \frac{k_s + 2k_f + 2(k_s - k_f)(1 + \nu)^3\phi}{k_s + 2k_f - 2(k_s - k_f)(1 + \nu)^3\phi}. \end{cases} \quad (5)$$

In Eq. (5),  $\rho_f$  and  $\rho_s$  denote the density of the base fluid and the nanoparticles, respectively,  $\mu_f$  denotes the viscosity of the base fluid,  $(c_p)_f$  and  $(c_p)_s$  denote the heat capacity of the base fluid and the nanoparticles, respectively,  $\sigma_f$  and  $\sigma_s$  denote the electrical conductivity of the base fluid and the nanoparticles, respectively, while  $k_f$  and  $k_s$  denote the thermal conductivities of the base fluid and the nanoparticles, respectively.  $\nu$  is a non-dimensional quantity, giving the ratio between the thickness of the nanolayer and the radius of the nanoparticle. The net external body force  $F_B$  may be expressed as

$$F_B = \rho_e E + J \times B, \quad (6)$$

where  $\rho_e$  represents the net charge density. Considering Hall current and using the generalized Ohm's law<sup>[31]</sup>, the electric current density  $J$  may be defined by

$$J + \frac{\sigma_{nf}}{en_e}(J \times B) = \sigma_{nf}(E + u \times B), \quad (7)$$

where  $e$  is the fundamental charge of an electron, and  $n_e$  is the number density of free electrons. Assuming that the applied magnetic field considered in the present study is sufficiently strong, we shall investigate the impact of the Hall current on fluid flow and heat transfer, because the current density and Lorentz force are both significantly affected by Hall current. The Hall parameter can be measured by the ratio of electron-cyclotron frequency and electron atom collision frequency. It is negligible only when the applied magnetic field is not strong or electron collision frequency is low. Considering the Rosseland approximation<sup>[32]</sup>, the heat flux  $q$  may be expressed as  $q = -4\sigma^* \nabla T^4 / (3k^*)$ , in which  $\sigma^*$  represents Stefan-Boltzmann constant, and  $k^*$  represents the absorption coefficient of the nanofluid. Expanding  $T^4$  in Taylor's series about the wall temperature  $T_w$  and ignoring higher order terms beyond first degree, we may write  $T^4 \approx 4T_w^3 T - 3T_w^4$ . Therefore, the divergence of the heat flux vector  $q$  becomes

$$\nabla \cdot q = -\frac{16\sigma^* T_w^3}{3k^*} \nabla^2 T. \quad (8)$$

## 2.2 EDL

It is known that when an ionized solution is in contact with the walls of a dielectric microchannel, an EDL is formed in the neighborhood of the wall. It consists of two layers of oppositely charged ions. The layer in the immediate vicinity of the wall is called stern layer that contains ions, which have the dimension of one atomic diameter. In the diffuse layer, next to the stern layer, a thermal motion is set up caused by the free migration of counter ions. A zeta potential is developed between the two layers. Its value may not be a constant, if the geometry of the microchannel walls is non-uniform. In order to determine an explicit form of the charge density  $\rho_e$  that appears in Eq. (6), let us use the following Poisson equation<sup>[33–34]</sup>, which relates the electrical potential  $\psi^*$  with the total ionic charge density  $\rho_e$  as

$$\nabla^2 \psi^* = -\rho_e / \epsilon_{nf}. \quad (9)$$

For a  $\varsigma : \varsigma$  symmetric electrolyte, we can express the total ionic charge density as  $\rho_e = e\varsigma(n^+ - n^-)$ ,  $n^+$  and  $n^-$  are respectively the co-ion and counter-ion number densities within the EDL. Following the Boltzmann distribution, we may write  $n^\pm = n_0 \exp(\mp e\varsigma\psi^* / (k_B T_{av}))$ , where  $n_0$  is the ionic concentration,  $\varsigma$  is the ionic valancy,  $k_B$  is the Boltzmann constant, and  $T_{av}$  the absolute temperature of the capillary. In Eq. (9),  $\epsilon_{nf}$  is the effective permittivity of the medium defined for the composite medium by the relation<sup>[35]</sup>

$$\frac{\epsilon_{nf}}{\epsilon_f} = 1 + \frac{2(\epsilon_s - \epsilon_f)\phi}{(\epsilon_s + 2\epsilon_f) - \phi(\epsilon_s - \epsilon_f)}. \quad (10)$$

We assume that the surface potential ( $\psi^*$ ) is a constant ( $\psi^* = \zeta_0^*$ ). Further, assuming that the surface zeta potential is very small ( $|\zeta_0^*| \leq 25$  mV), we use the Debye-Hückel approximation, which transforms the net charge densities of ion in a unit volume of fluid as  $n^\pm = n_0(1 \mp e\zeta\psi^*/(k_B T_{av}))$ . In order to obtain a non-dimensional form of Eq. (9), we introduce the dimensionless quantities as

$$\psi = \psi^*/\zeta_0^*, \quad \eta = \eta^*/d^*, \quad \xi = \xi^*/L, \quad h = H^*/d^*. \quad (11)$$

Further, using the aforesaid assumption  $2H^* \ll W \ll L$ , Eq. (9) reduces to the following form:

$$\frac{\epsilon_{nf}}{\epsilon_f} \frac{d^2\psi}{d\eta^2} = \kappa^2 \psi. \quad (12)$$

Solving Eq. (12) subject to the conditions on the following boundaries:

$$\begin{cases} \frac{d\psi}{d\eta} = 0 & \text{at } \eta = 0, \\ \psi = 1 & \text{at } \eta = h = 1 - a \cos^2(\pi\xi), \end{cases} \quad (13)$$

we may write the expression of net charge density  $\rho_e$  as follows:

$$\rho_e = -\frac{\epsilon_f \zeta_0^* \cosh(\kappa\eta/\varepsilon)}{\lambda_D^2 \cosh(\kappa h/\varepsilon)}, \quad (14)$$

where  $\kappa = d^*/\lambda_D$  is the Debye-Hückel parameter,  $\lambda_D = \sqrt{\epsilon_f k_B T_{av}/(2n_0 e^2 \zeta^2)}$  is the Debye length,  $\varepsilon^2 = \epsilon_{nf}/\epsilon_f$ , and  $a = a^*/d^*$  is the dimensionless amplitude of the wavy walls. It is noteworthy that the distribution of ions will be affected by the action of the external magnetic field. The electrical potential distribution will then be reflected in the whole system. However, in this study, the effect of magnetic field on the EDL has been neglected in view of the fact that the electromagnetic induction under magnetic environment is negligibly small<sup>[36]</sup>.

### 2.3 Velocity distribution

If the Reynolds number is small, the microfluidic transport of the fluid happens to be slow and usually it takes place unidirectionally. In the analysis that follows, velocities in the  $\chi^*$ - and  $\eta^*$ -directions will be ignored, i.e.,  $v^* \approx 0$ ,  $w^* \approx 0$ . Moreover, since in the present problem, the magnetic Reynolds number  $Re_m = v_{ref} l_{ref}/v_m$  ( $v_{ref}$  is the reference velocity,  $l_{ref}$  is the reference length, and  $v_m$  is the magnetic diffusivity) is small, the magnetic induction is negligibly small. Then, the Navier-Stokes equation given by Eq. (3), that describes the velocity of the nanofluid, reduces to

$$-\frac{dp^*}{d\xi^*} + \mu_{nf} \left( \frac{\partial^2 u^*}{\partial \eta^{*2}} - \frac{u^*}{k^*} \right) + \rho_e E_\xi = \frac{\sigma_{nf} B_0^2 u^*}{1 + m_{nf}^2} - \frac{\sigma_{nf} m_{nf} B_0 E_\xi}{1 + m_{nf}^2}, \quad (15)$$

in which  $m_{nf} = \sigma_{nf} B_0/(en_e)$  represents the effective Hall parameter for the nanofluid. It is known that no-slip boundary conditions are not valid for problems of physiological flow of blood in arteries and heart valves, rarefield fluid motion, and thin films. Thompson and Troian<sup>[37]</sup> observed that a thin film is formed along the walls of a capillary, when a dilute suspension of particles flows through it. In view of all these, the velocity-slip boundary conditions at the walls of the capillary together with the conditions of symmetry about the central-line of the capillary need to be considered for solving the present problem that deals with flow of fluids containing nanoparticles. These conditions may be put mathematically as

$$\begin{cases} \frac{\partial u^*}{\partial \eta^*} = 0 & \text{at } \eta^* = 0, \\ u^* + \beta^* \frac{\partial u^*}{\partial \eta^*} = 0 & \text{at } \eta^* = H^*. \end{cases} \quad (16)$$

The boundary condition is known as the Navier slip boundary condition, where  $\beta^*$  is the slip length. It is worthwhile to note here that in the absence of slip length,  $\beta^* = 0$ . In this case, Navier slip boundary condition truncates to the no-slip boundary condition, while relatively larger values ( $\beta^* \rightarrow \infty$ ) yield the surface traction boundary condition.

On introducing non-dimensional velocity  $u = u^*/u_{\text{HS}}$ , where  $u_{\text{HS}} = -\zeta_0^* \epsilon_f E_0 / \mu_f$  is the Helmholtz-Smoluchowski velocity with  $E_0$  as the strength of characteristic electric field and making use of the non-dimensional variables mentioned above, we obtain

$$\frac{\mu_{\text{nf}}}{\mu_f} \left( \frac{\partial^2 u}{\partial \eta^2} - \frac{u}{Da} \right) + E_s \kappa^2 \frac{\cosh(\kappa \eta / \varepsilon)}{\cosh(\kappa h / \varepsilon)} + \Gamma = \frac{\sigma_{\text{nf}} Ha^2 u}{\sigma_f (1 + m_{\text{nf}}^2)} - \frac{\sigma_{\text{nf}} m_{\text{nf}} Ha S E_s}{\sigma_f (1 + m_{\text{nf}}^2)}, \quad (17)$$

in which  $Da = k^*/d^{*2}$  represents the Darcy number,  $E_s = E_\xi / E_0$ ,  $Ha = \sqrt{\sigma_f / \mu_f} d^* B_0$  represents the Hartmann number,  $m = \sigma_f B_0 / (en_e)$  is the Hall parameter,  $\Gamma = (-dp^*/d\xi^*) d^{*2} / (\mu_f u_{\text{HS}})$  is a dimensionless parameter denoting the strength ratio of pressure driven velocity and electroosmotic velocity, and  $S = \sqrt{\sigma_f / \mu_f} E_0 d^* / u_{\text{HS}}$  stands for the characteristic electric field intensity in its non-dimensional form. It may be mentioned that  $\Gamma > 0$  corresponds to pressure assisting flow, while  $\Gamma < 0$  stands for the pressure opposing flow. When  $\Gamma = 0$ , we have the case of purely magnetohydrodynamic flow. Using the aforesaid dimensionless variables, boundary condition (16) may be rewritten as

$$\begin{cases} \frac{\partial u}{\partial \eta} = 0 & \text{at } \eta = 0, \\ u + \beta \frac{\partial u}{\partial \eta} = 0 & \text{at } \eta = h, \end{cases} \quad (18)$$

in which the parameter  $\beta = \beta^*/d^*$  takes care of the slip velocity. Now, solving Eq. (17) subject to the conditions (18), we obtain

$$\begin{aligned} u(\xi, \eta) = & \frac{\mu_f}{\mu_{\text{nf}}} \left( \frac{\Gamma}{\alpha^2} - \frac{\sigma_{\text{nf}}}{\sigma_f} \frac{m_{\text{nf}} Ha S E_s}{\alpha^2 (1 + m_{\text{nf}}^2)} \right) \left( 1 - \frac{\cosh(\alpha \eta)}{a_1 \cosh(\alpha h)} \right) \\ & + \frac{\mu_f}{\mu_{\text{nf}}} \frac{E_s \kappa^2 \varepsilon^2}{(\kappa^2 - \alpha^2 \varepsilon^2)} \left( \frac{a_2 \cosh(\alpha \eta)}{a_1 \cosh(\alpha h)} - \frac{\cosh(\kappa \eta / \varepsilon)}{\cosh(\kappa h / \varepsilon)} \right), \end{aligned} \quad (19)$$

where  $\alpha = \sqrt{\frac{(\sigma_{\text{nf}}/\sigma_f) Ha^2}{(\mu_{\text{nf}}/\mu_f)(1+m_{\text{nf}}^2)}} + \frac{1}{Da}$ ,  $a_1 = 1 + \alpha \beta \tanh(\alpha h)$ , and  $a_2 = 1 + \frac{\kappa \beta}{\varepsilon} \tanh(\kappa h / \varepsilon)$ . The skin friction on the microchannel surface is given by

$$C_f = \frac{d^*}{\mu_f u_{\text{HS}}} \tau_{\xi^* \eta^*} \Big|_{\eta^* = H^*} = - \frac{\mu_{\text{nf}}}{\mu_f} \frac{\partial u}{\partial \eta} \Big|_{\eta = h}. \quad (20)$$

## 2.4 The streaming potential

As we know, streaming potential is the potential difference that arises across a channel or a membrane, when a liquid flows on it. Equation (19) gives the resultant of the pressure-driven velocity and the velocity generated by the streaming current. The second term on the right side of this equation contributes to the resistance to flow caused due to streaming potential. As indicated earlier, the electric field in the system generates a conduction current in a direction opposite to that of the streaming current. However, on the surface of the channel the net ionic current is zero<sup>[33]</sup>, i.e.,

$$I = 2e\varsigma \int_0^{H^*} (n^+ u_+ - n^- u_-) d\eta^* = I_s + I_c = 0, \quad (21)$$

where  $I_s$  and  $I_c$  respectively denote the streaming current and conduction current.  $u_{\pm}$  refer to the ionic velocities, which may be expressed as  $u_{\pm} = u^* \pm \frac{e\varsigma E_\xi}{f_{\pm}}$ , with  $f_{\pm}$  as the ionic

friction coefficients, for co-ion and counter-ion, respectively. Making use of the aforesaid non-dimensional quantities in Eq. (21), we finally obtain the expression of non-dimensional streaming potential  $E_s$  in the form

$$E_s = \frac{\Gamma b_1}{\alpha^2} \left/ \left( \frac{\sigma_{nf}}{\sigma_f} \frac{m_{nf} H a S b_1}{\alpha^2 (1 + m^2)} - \frac{\kappa^2 \varepsilon^2 b_2}{\kappa^2 - \alpha^2 \varepsilon^2} + \frac{\mu_{nf}}{\mu_f} R h \cosh(\kappa h / \varepsilon) \right) \right., \quad (22)$$

in which  $R = \frac{k_B T_{av} E_0}{f w_{HS}}$ ,  $b_1 = \varepsilon \sinh(\kappa h / \varepsilon) - \frac{b_3}{2a_1} \text{sech}(\alpha h)$ ,  $b_2 = \frac{a_2 b_3}{2a_1} \text{sech}(\alpha h) - \frac{b_4}{2} \text{sech}(\kappa h / \varepsilon)$ ,  $b_3 = \frac{\varepsilon}{\alpha \varepsilon + \kappa} \sinh\left((\alpha + \frac{\kappa}{\varepsilon})h\right) + \frac{\varepsilon}{\alpha \varepsilon - \kappa} \sinh\left((\alpha - \frac{\kappa}{\varepsilon})h\right)$ , and  $b_4 = h + \frac{\varepsilon}{2\kappa} \sinh\left(\frac{2\kappa h}{\varepsilon}\right)$ . Equation (22) provides an estimate of the streaming potential.

## 2.5 Temperature distribution

The main objective of the present analysis is to study the effect of nanoparticles on thermal transport mechanism associated with electromagnetohydrodynamic flow through a capillary during chemotherapy. Based on the geometry of the present problem, let us examine the energy distribution during fluid flow, considering the velocity distribution given by Eq. (19), along with volumetric joule heating and energy dissipation factor. The effects of both thermal radiation and external magnetic field on temperature distribution are accounted for. Moreover, the presence of a constant heat flux  $q_w$  through the wavy walls of the capillary is considered in the present analysis. In view of all the above considerations, the governing equation for thermal energy is found to be given by

$$(\rho c_p)_{nf} u^* \frac{\partial T}{\partial \xi^*} = \left( k_{nf} + \frac{16\sigma^* T_w^3}{3k^*} \right) \left( \frac{\partial^2 T}{\partial \xi^{*2}} + \frac{\partial^2 T}{\partial \eta^{*2}} \right) + \frac{\sigma_{nf}(E_\xi^2 + B_0^2 u^{*2})}{1 + m_{nf}^2} + \mu_{nf} \left( \frac{\partial u^*}{\partial \eta^*} \right)^2. \quad (23)$$

The second term in the right side of Eq. (23) is concerned with the volumetric heat generation due to external body forces while the last term represent local volumetric heat generation due to viscous dissipation. For the present problem, Eq. (23) needs to be solved subject to the uniform heat flux boundary condition, considering temperature jump. Thus, the boundary conditions may be expressed mathematically as

$$\begin{cases} \frac{\partial T}{\partial \eta^*} = 0 & \text{at } \eta^* = 0, \\ T + \delta^* \frac{\partial T}{\partial \eta^*} = T_w, \\ k_{nf} \frac{\partial T}{\partial \eta^*} = q_w & \text{at } \eta^* = H^*, \end{cases} \quad (24)$$

where  $\delta^*$  is the hight of temperature jump, and  $q_w = h_f(T_w - T_m)$  accounts for the uniform heat flux applied throughout the entire upper wall of the channel considered here,  $h_f$  stands for the convective heat transfer coefficient,  $T_w$  stands for the wall temperature, while  $T_m$  represents the bulk mean temperature defined as  $T_m = \int_0^{H^*} u^* T d\eta^* / (\int_0^{H^*} u^* d\eta^*)$ . Considering the axial invariance of the fluid temperature and uniformity of wall heat flux, we take  $\frac{\partial T}{\partial \xi^*} = \frac{dT_w}{d\xi^*} = \frac{dT_m}{d\xi^*} = \text{constant}$ , so that  $\frac{\partial^2 T}{\partial \xi^{*2}} = 0$ . Under these considerations, Eq. (23) may be rewritten as follows:

$$(\rho c_p)_{nf} u^* \frac{dT_m}{d\xi^*} = \left( k_{nf} + \frac{16\sigma^* T_w^3}{3k^*} \right) \frac{\partial^2 T}{\partial \eta^{*2}} + \frac{\sigma_{nf}(E_\xi^2 + B_0^2 u^{*2})}{1 + m_{nf}^2} + \mu_{nf} \left( \frac{\partial u^*}{\partial \eta^*} \right)^2. \quad (25)$$

In order to determine the axial bulk mean temperature gradient, let us apply the global energy balance equation on Eq. (25) by considering over energy balance for an element control volume



on a length  $d\xi^*$  at the central line of the channel<sup>[4]</sup>. Then, we have

$$\begin{aligned} \int_0^{H^*} (\rho c_p)_{\text{nf}} u^* dT_m d\eta^* &= \int_0^{H^*} \left( k_{\text{nf}} + \frac{16\sigma^* T_w^3}{k^*} \right) \frac{\partial^2 T}{\partial \eta^{*2}} d\xi^* d\eta^* + \int_0^{H^*} \frac{\sigma_{\text{nf}} E_\xi^2}{1 + m_{\text{nf}}^2} d\xi^* d\eta^* \\ &+ \int_0^{H^*} \frac{\sigma_{\text{nf}} B_0^2 u^{*2}}{1 + m_{\text{nf}}^2} d\xi^* d\eta^* + \int_0^{H^*} \mu_{\text{nf}} \left( \frac{\partial u^*}{\partial \eta^*} \right)^2 d\xi^* d\eta^*. \end{aligned} \quad (26)$$

Using the uniform heat flux boundary condition in Eq. (26), we obtain the expression of axial bulk mean temperature gradient for fully thermally developed flow as

$$\frac{dT_m}{d\xi^*} = \frac{(1 + (N_r)_{\text{nf}})q_w}{(\rho c_p)_{\text{nf}} u_{\text{av}}} + \frac{\sigma_{\text{nf}}(E_\xi^2 H^* + B_0^2 I_1)}{(\rho c_p)_{\text{nf}} u_{\text{av}}(1 + m_{\text{nf}}^2)} + \frac{\mu_{\text{nf}} I_2}{(\rho c_p)_{\text{nf}} u_{\text{av}}}, \quad (27)$$

where  $(N_r)_{\text{nf}} = \frac{N_r}{k_{\text{nf}}/k_f}$  is the effective thermal radiation parameter of the nanofluid,  $N_r = \frac{16\sigma^* T_w^3}{k^* k_f}$ ,  $u_{\text{av}} = \int_0^{H^*} u^* d\eta^* = u_{\text{HS}} d^* \beta_1$ ,  $I_1 = \int_0^{H^*} (u^*)^2 d\eta^* = d^* \beta_2 u_{\text{HS}}^2$ , and  $I_2 = \int_0^{H^*} \left( \frac{\partial u^*}{\partial \eta^*} \right)^2 d\eta^* = \frac{\beta_3 u_{\text{HS}}^2}{d^*}$ , in which

$$\begin{aligned} \beta_1 &= \frac{\mu_f}{\mu_{\text{nf}}} \left( c_0 \left( h - \frac{\tanh(\alpha h)}{\alpha a_1} \right) + \frac{\kappa \varepsilon^2 E_s}{a_1 (\kappa^2 - \alpha^2 \varepsilon^2)} \left( \frac{\kappa \tanh(\alpha h)}{\alpha} - \frac{\varepsilon}{\coth(\kappa h/\varepsilon)} \right) \right), \\ \beta_2 &= \left( \frac{\mu_f}{\mu_{\text{nf}}} \right)^2 c_0^2 h + \frac{c_1^2}{2} \left( h + \frac{\sinh(2\alpha h)}{2\alpha} \right) + \frac{\mu_f}{\mu_{\text{nf}}} c_0 \left( \frac{2c_1}{\alpha} \sinh(\alpha h) - \frac{2c_2 \varepsilon}{k} \sinh(\kappa h/\varepsilon) \right) \\ &+ c_2^2 b_4 - c_1 c_2 b_3, \\ \beta_3 &= \frac{\alpha^2 c_1^2}{2} \left( \frac{\sinh(2\alpha h)}{2\alpha} - h \right) + \frac{\varepsilon^2 c_2^2}{\kappa^2} \left( \frac{\varepsilon}{2\kappa} \sinh(2\kappa h/\varepsilon) - h \right) \\ &- \frac{\alpha \varepsilon c_1 c_2}{\kappa} \left( \frac{\varepsilon}{\alpha \varepsilon + \kappa} \sinh \left( \left( \alpha + \frac{\kappa}{\varepsilon} \right) h \right) - \frac{\varepsilon}{\alpha \varepsilon - \kappa} \sinh \left( \left( \alpha - \frac{\kappa}{\varepsilon} \right) h \right) \right), \\ c_0 &= \left( \frac{\Gamma}{\alpha^2} - \frac{\sigma_{\text{nf}}}{\sigma_f} \frac{E_s H a S m_{\text{nf}}}{\alpha^2 (1 + m_{\text{nf}}^2)} \right), \\ c_1 &= \frac{\mu_f}{\mu_{\text{nf}}} \left( \frac{\kappa^2 \varepsilon^2 a_2 E_s}{a_1 (\kappa^2 - \varepsilon^2 \alpha^2)} - \frac{\Gamma}{\alpha^2 a_1} + \frac{\sigma_{\text{nf}}}{\sigma_f} \frac{m_{\text{nf}} H a S E_s}{\alpha^2 (1 + m_{\text{nf}}^2)} \right) \text{sech}(\alpha h), \\ c_2 &= \frac{\mu_f}{\mu_{\text{nf}}} \frac{\kappa^2 \varepsilon^2 E_s}{a_1 (\kappa^2 - \alpha^2 \varepsilon^2)} \text{sech}(\kappa h/\varepsilon). \end{aligned}$$

On introducing the classical non-dimensional temperature  $\Theta = \frac{T - T_w}{\frac{q_w d^*}{k_f}}$  and using Eq. (27) in Eq. (25), we obtain the non-dimensional form of energy equation as follows:

$$\left( \frac{k_{\text{nf}}}{k_f} + N_r \right) \frac{\partial^2 \Theta}{\partial \eta^2} = \frac{A u}{\beta_1} - \frac{\sigma_{\text{nf}}}{\sigma_f} \frac{\varrho E_s^2 + H a^2 Br u^2}{1 + m_{\text{nf}}^2} - \frac{\mu_{\text{nf}}}{\mu_f} Br \left( \frac{\partial u}{\partial \eta} \right)^2, \quad (28)$$

where  $A = (1 + (N_r)_{\text{nf}}) + \frac{\sigma_{\text{nf}}}{\sigma_f} \frac{\varrho E_s^2 + H a^2 Br \beta_2}{1 + m_{\text{nf}}^2} + \frac{\mu_{\text{nf}}}{\mu_f} Br \beta_3$ ,  $\varrho = \frac{\sigma_f E_0^2 d^*}{q_w}$  is a measure of the Joule heating.  $Br = \frac{\mu_f u_{\text{HS}}^2}{d^* q_w}$  is called the Brinkman number. The constant axial temperature gradient may be put in its non-dimensional form as

$$\frac{\partial \Theta}{\partial \xi} = \frac{(\rho c_p)_f}{(\rho c_p)_{\text{nf}}} \frac{1}{Pe} \left( \frac{1 + (N_r)_{\text{nf}}}{\beta_1} + \frac{\sigma_{\text{nf}}}{\sigma_f} \frac{\varrho E_s^2 h}{(1 + m_{\text{nf}}^2) \beta_1} + \frac{\sigma_{\text{nf}}}{\sigma_f} \frac{\beta_2 H a^2 Br}{(1 + m_{\text{nf}}^2) \beta_1} + \frac{\mu_{\text{nf}}}{\mu_f} Br \frac{\beta_3}{\beta_1} \right), \quad (29)$$

in which  $Pe = \frac{(\rho c_p)_f u_{\text{HS}} d^*}{k_f}$  stands for the Péclet number. The dimensionless form of symmetric

boundary condition together with the temperature jump condition given by Eq. (24) now reads

$$\begin{cases} \frac{\partial \Theta}{\partial \eta} = 0 & \text{at } \eta = 0, \\ \Theta + \delta \frac{\partial \Theta}{\partial \eta} = 0 & \text{at } \eta = h, \end{cases} \quad (30)$$

$\delta = \delta^*/d^*$  stands a measure of temperature jump. The solution to Eq. (28) subject to the condition (30) gives the dimensionless temperature distribution as

$$\Theta(\xi, \eta) = \frac{1}{\frac{k_{nf}}{k_f} + N_r} \left( \gamma + \frac{A f_1(\eta)}{\beta_1} - \frac{\sigma_{nf}/\sigma_f}{1 + m_{nf}^2} \left( \frac{\varrho E_s^2 \eta^2}{2} + H a^2 B r f_2(\eta) \right) - \frac{\mu_{nf}}{\mu_f} B r f_3(\eta) \right), \quad (31)$$

in which

$$\begin{aligned} \gamma &= \frac{\sigma_{nf} \varrho E_s^2}{\sigma_f (1 + m_{nf}^2)} \left( \frac{h^2}{2} + \delta h \right) + \frac{\sigma_{nf} H a^2 B r}{\sigma_f (1 + m_{nf}^2)} (f_2(h) + \delta \beta_2) \\ &\quad + \frac{\mu_f}{\mu_{nf}} B r (f_3(h) + \delta \beta_3) - A \left( \delta + \frac{f_1(h)}{\beta_1} \right), \\ f_1(\eta) &= \frac{\mu_f}{\mu_{nf}} \frac{c_0 \eta^2}{2} + \frac{c_1}{\alpha^2} \cosh(\alpha \eta) - \frac{\varepsilon c_2}{\kappa^2} \cosh(\kappa \eta / \varepsilon), \\ f_2(\eta) &= \left( \frac{\mu_f}{\mu_{nf}} \right)^2 \frac{c_0^2 \eta^2}{2} + \frac{c_1^2}{2} \left( \frac{\eta^2}{2} + \frac{\cosh(2\alpha \eta)}{4\alpha^2} \right) + \frac{c_2^2}{2} \left( \frac{\eta^2}{2} + \frac{\varepsilon^2 \cosh(2\kappa \eta / \varepsilon)}{4\kappa^2} \right) + \frac{2c_0 c_1}{\alpha^2} \cosh(\alpha \eta) \\ &\quad - c_1 c_2 \left( \frac{\varepsilon^2}{(\alpha \varepsilon + \kappa)^2} \cosh \left( \left( \alpha + \frac{\kappa}{\varepsilon} \right) \eta \right) + \frac{\varepsilon^2}{(\alpha \varepsilon - \kappa)^2} \cosh \left( \left( \alpha - \frac{\kappa}{\varepsilon} \right) \eta \right) \right), \\ f_3(\eta) &= \frac{\alpha^2 c_1^2}{2} \left( \frac{\cosh(2\alpha \eta)}{4\alpha^2} - \frac{\eta^2}{2} \right) + \frac{\kappa^2 c_2^2}{\varepsilon^2} \left( \frac{\varepsilon^2 \cosh(2\kappa \eta / \varepsilon)}{4\kappa^2} - \frac{\eta^2}{2} \right) \\ &\quad - \frac{\kappa \alpha c_1 c_2}{\varepsilon} \left( \frac{\varepsilon^2}{(\alpha \varepsilon + \kappa)^2} \cosh \left( \left( \alpha + \frac{\kappa}{\varepsilon} \right) \eta \right) - \frac{\varepsilon^2}{(\alpha \varepsilon - \kappa)^2} \cosh \left( \left( \alpha - \frac{\kappa}{\varepsilon} \right) \eta \right) \right). \end{aligned}$$

Having determined the axial velocity and temperature as in Eq. (19) and Eq. (31), respectively, we now proceed to determine some physical quantities that are of prime importance for heat transfer analysis, e.g., the bulk mean temperature and the heat transfer coefficient. The non-dimensional bulk mean temperature for the present study is given by

$$\Theta_m = \frac{\int_0^h u \Theta d\eta}{\int_0^h u d\eta} = \frac{k_f (T_m - T_w)}{q_w d^*}. \quad (32)$$

Further the Nusselt number may be expressed as  $Nu = \frac{q_w d^*}{k_{nf} (T_w^* - T_m^*)}$ . Now, using Eq. (32), we obtain the Nusselt number in the form

$$Nu = - \frac{k_f}{k_{nf}} \frac{1}{\Theta_m}. \quad (33)$$

## 2.6 Entropy generation analysis

Considering that entropy generation is of utmost concern, while investigating the thermodynamical behavior of a system, we now intend to perform the entropy generation analysis for the problem under consideration as Bejan<sup>[23]</sup>. The volumetric rate of local entropy generation may be determined by using the following equation<sup>[16,38]</sup>:

$$S_G^* = (k_{nf} \nabla T - q) \cdot \frac{\nabla T}{T_w^2} + \frac{1}{\sigma_{nf} T_w} J \cdot J + \frac{1}{T_w} \boldsymbol{\tau} \cdot \nabla u + \frac{\mu_{nf}}{k^* T_w} u \cdot u, \quad (34)$$

where  $S_G^*$  represents the total volumetric entropy generation rate per unit volume. For unidirectional flows, using the conditions mentioned in Subsection 2.3, we can write

$$S_G^* = S_T^* + S_J^* + S_M^* + S_F^* + S_P^*, \quad (35)$$

where

$$\begin{aligned} S_T^* &= \frac{1}{T_w^2} \left( k_{nf} + \frac{16\sigma^* T_w^3}{3k^*} \right) \left( \left( \frac{\partial T}{\partial \xi^*} \right)^2 + \left( \frac{\partial T}{\partial \eta^*} \right)^2 \right), & S_J^* &= \frac{\sigma_{nf} E_\xi^2}{T_w(1 + m_{nf}^2)}, \\ S_M^* &= \frac{\sigma_{nf} B_0^2 u^{*2}}{T_w(1 + m_{nf}^2)}, & S_F^* &= \frac{\mu_{nf}}{T_w} \left( \frac{\partial u^*}{\partial \eta^*} \right)^2, & S_P^* &= \frac{\mu_{nf} u^{*2}}{T_w k^*}, \end{aligned}$$

which represent, respectively, the thermoradiative heat transfer irreversibility, the Joule heating irreversibility, the magnetic field irreversibility, the fluid flow irreversibility, and the porosity irreversibility, respectively. Introducing the following physical constant that represents the entropy generation rate,

$$S_G^o = k_f \left( \frac{q_w d^*}{k_f} \right)^2 / (T_w^2 d^{*2}), \quad (36)$$

dimensionless volumetric entropy generation is given by

$$\begin{aligned} S_G = \frac{S_G^*}{S_G^o} &= \frac{k_{nf}}{k_f} (1 + (N_r)_{nf}) \left( \left( \frac{\partial \Theta}{\partial \xi} \right)^2 + \left( \frac{\partial \Theta}{\partial \eta} \right)^2 \right) + \frac{\sigma_{nf}}{\sigma_f} \frac{\varrho E_s^2}{\Re(1 + m_{nf}^2)} \\ &+ \frac{\sigma_{nf}}{\sigma_f} \frac{Ha^2 Br}{\Re(1 + m_{nf}^2)} \frac{u^2}{\Re} + \frac{\mu_{nf}}{\mu_f} \frac{Br}{\Re} \left( \frac{\partial u}{\partial \eta} \right)^2 + \frac{\mu_{nf}}{\mu_f} \frac{Br}{\Re} \frac{u^2}{Da}, \end{aligned} \quad (37)$$

where  $\Re = \frac{q_w d^*/k_f}{T_w}$  is a dimensionless temperature difference parameter. Alternatively the thermal irreversibility of the system can be calculated from Bejan number<sup>[39]</sup>, which is the ratio of the heat transfer irreversibility to total irreversibility of the system. Mathematically,

$$Be = \frac{S_T^*}{S_G^*} = \frac{k_{nf}}{k_f} \frac{(1 + (N_r)_{nf})}{S_G} \left( \left( \frac{\partial \Theta}{\partial \xi} \right)^2 + \left( \frac{\partial \Theta}{\partial \eta} \right)^2 \right). \quad (38)$$

The maximum and minimum values of  $Be$  are respectively 1 and 0. When only heat transfer dominates over total irreversibility,  $Be = 1$ . But when the resultant effect of irreversibility caused by Joule heating, fluid friction, medium porosity, and magnetic field, the value of Bejan number is zero; if for entropy generation, the contribution of heat transfer is equal to the resultant effect of fluid friction, medium porosity, magnetic field, and Joule heating, the value of  $Be$  is 0.5.

Thus,

$$Be = \begin{cases} 0 & \text{if } S_J^* + S_M^* + S_F^* + S_P^* = S_G^*, \\ 1/2 & \text{if } S_J^* + S_M^* + S_F^* + S_P^* = S_T^*, \\ 1 & \text{if } S_J^* + S_M^* + S_F^* + S_P^* = 0. \end{cases} \quad (39)$$

### 3 Results and discussion

In the previous section, we derive analytical expression of the axial velocity, streaming potential, temperature profile, and Nusselt number. In this section, we discuss the effects of various non-dimensional parameters on the axial velocity, streaming potential, temperature profile, and Nusselt number in case of fluid flow in the micro-circulatory system.

### 3.1 Estimation of the involved parameters

In order to calculate numerical estimates, we consider values of different physical constants involved in the present study, as given in Table 2. Using the value of  $\mu_f$  given in Table 2 and considering the formulae  $u_{HS} = -\zeta_0^* \epsilon_f E_0 / \mu_f$  and  $R = \frac{k_B T_{av} E_0}{\zeta_0^* f u_{HS}}$  as in Eq. (22), we find

$$u_{HS} \approx 3 \times 10^{-2} \text{ m} \cdot \text{s}^{-1}, \quad R \approx -0.5.$$

It may be mentioned here that the magnetic field strength 8 T considered in the present study is strong enough for the orientation of erythrocytes of blood, as per the observation of an experimental report of Higashi et al.<sup>[40]</sup>.

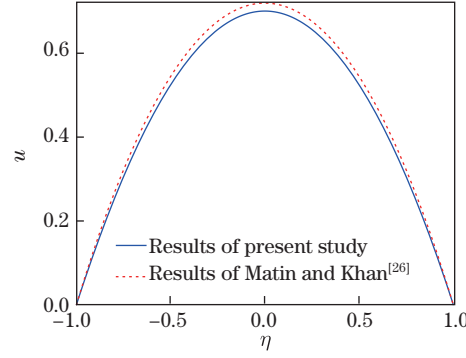
**Table 2** Typical values of physical parameters<sup>[14–15,35,39]</sup>

Parameter	Symbol	Value	Unit
Half channel height	$d^*$	50	$\mu\text{m}$
Amplitude of the channel	$a^*$	1–5	$\mu\text{m}$
Charge of electron	$e$	$1.6 \times 10^{-19}$	C
Boltzmann constant	$k_B$	$1.38 \times 10^{-23}$	$\text{J} \cdot \text{K}^{-1}$
Channel length	$L$	0.005	m
Ionic concentration	$n_0$	1	$\text{mol} \cdot \text{m}^{-3}$
Average absolute temperature	$T_{av}$	300	K
Viscosity	$\mu_f$	$3.2 \times 10^{-3}$	$\text{Pa} \cdot \text{s}$
Ionic valency	$\varsigma$	1	—
Electric potential	$\zeta_0^*$	−0.025	V
Strength of characteristics electric field	$E_0$	0–20	$\text{kV} \cdot \text{m}^{-1}$
Permeability of capillary	$k^*$	0.4	$\mu\text{m}^2$
Magnetic field strength	$B_0$	0–8	T
Ionic friction coefficient	$f$	$10^{-12}$	$\text{N} \cdot \text{s} \cdot \text{m}^{-1}$
Slip length	$\beta^* / \delta^*$	1–300	nm
Stefan-Boltzmann constant	$\sigma^*$	$5.67 \times 10^{-8}$	$\text{W} \cdot \text{m}^2 \cdot \text{K}^{-4}$
Absorption coefficient of nanofluid	$k^*$	$10^{-1}$	$\text{m}^{-1}$
Wall heat flux	$q_w$	1 500	$\text{W} \cdot \text{m}^{-2}$
A non-dimensional quantity	$\nu$	0.1	—

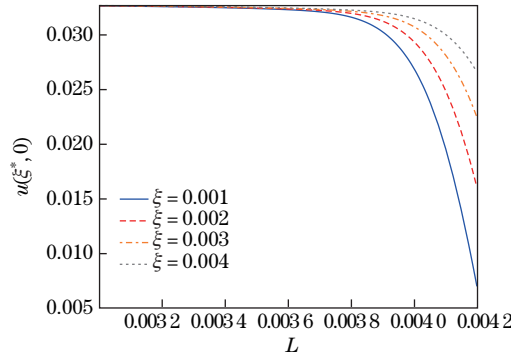
Figure 2 gives the velocity distribution of the nanofluid for the present study. We have also compared our results with those of the analytical study performed by Matin and Khan<sup>[26]</sup>, which have also been presented in the same figure. For the sake of a meaningful comparison, the results of the present study presented in Fig. 2, were computed by taking  $a = 0, \phi = 0, Ha = 0, \kappa = 10, \Delta p = 1, \beta = 0, R = -0.5$  and by considering the Darcy number to be large ( $Da \approx 10^3$ ). The results presented here correspond to pressure assisting flow, where  $\Gamma > 0$ . The two plots presented in Fig. 2 show that our results are in good agreement with those of Ref. [26].

### 3.2 Velocity distribution and skin friction

Figure 3 illustrates the effect of channel length on the central line velocity at different locations of the microchannel. In the physiological system, blood flow takes place in vessels of different length, varying from large arteries to capillaries. Keeping this in mind, we have examined the variation in electrokinetic velocity along the central line at different axial distances/channel lengths. The different graphs presented in Fig. 3 show that the electrokinetic velocity reduces with increase in channel length. However, as in real blood flow the velocity is maximum in the vicinity of the electrode.



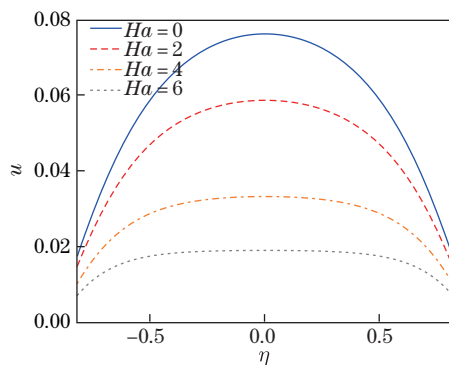
**Fig. 2** Comparison of velocity in the present study with that of Ref. [26] when  $a = \phi = Ha = \beta = 0$ ,  $\kappa = 10$ ,  $\Gamma = 1$ ,  $Da = 10^3$ , and  $R = -0.5$  (color online)



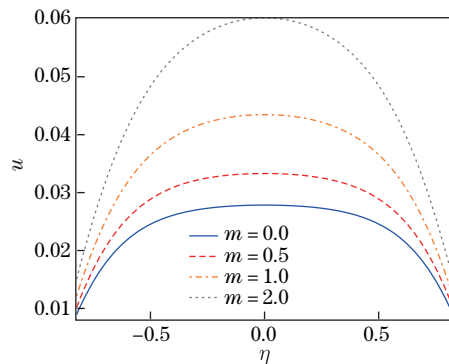
**Fig. 3** Variations in central line velocity as a function of channel length at different axial distances of the microchannel, when  $a = 0.05$ ,  $\phi = 0.05$ ,  $m = 0.5$ ,  $\beta = 0.1$ ,  $\kappa = 10$ ,  $\Gamma = 1$ ,  $Ha = 4$ , and  $Da = 0.1$  (color online)

Figure 4 gives the velocity distribution in the capillary for different values of the Hartmann number ( $Ha$ ). This figure reveals that velocity is maximum in the absence of any external magnetic field and that as intensity of the magnetic field increases, there occurs a significant reduction in velocity. Interpreting physically, we find the externally imposed magnetic field generates Lorentz force that retards flow of the fluid. The magnitude of Lorentz force increases with increase in the magnetic field strength. Owing to this, the retarding effect on fluid flow keeps increasing, as the strength of the magnetic field is increased. Figure 4 shows that in the range of values of the Hartmann number considered in the present study, the flatness of the velocity increases, as the Hartmann number increases; it is highest when  $Ha = 6$ . The impact of Hall current on fluid velocity can be found from Fig. 5. This figure shows that as the Hall parameter increases, the fluid velocity is enhanced. The physics behind this observation is that the electrical conductivity of ferromagnetic nanoparticles mixed with base fluid reduces as the Hall parameter increases and thereby the magnetic damping effect reduces and as a result fluid velocity is enhanced. More precisely, the effective conductivity  $\frac{\sigma_{nf}}{1+m_{nf}^2}$  decreases with increasing values of  $m$ . This causes significant reduction in the damping effect on electrokinetic velocity  $u$ , affected by the Hartmann number  $Ha$ . Figure 6 depicts the change in velocity distribution for different values of the Darcy number. Figure 6 shows that with rise in permeability, the magnitude of the velocity increases. It may be explained that when permeability increases, more fluid can pass through the porous medium and so the velocity enhances. From our analysis, we further find that the fluid velocity is enhanced with the increase in slip velocity. The corresponding figure has not been presented here for the sake of brevity. However, velocity-slip

does not have much impact on velocity in the neighborhood of the capillary axis but near the wall of the capillary, the slip effect is significant. One may note that the effects of slip velocity at the wall and the EDL transport can considerably affect the streaming potential that bears the promise to influence the energy transport mechanism in the capillary. Further it reveals that with increase in velocity-slip, there may be detachment of the fluid particles and as a result kinetic energy of the fluid particles is likely to be enhanced, due to which significant increase in fluid velocity will take place.



**Fig. 4** Influence of Hartmann number on distribution of velocity when  $a = 0.05$ ,  $\xi = 0.4$ ,  $\phi = 0.05$ ,  $m = 0.5$ ,  $Da = 0.1$ ,  $\beta = 0.1$ ,  $\kappa = 10$ ,  $\Gamma = 1$ , and  $S = 5$  (color online)



**Fig. 5** Influence of Hall effect on distribution of velocity when  $a = 0.05$ ,  $\xi = 0.4$ ,  $\phi = 0.05$ ,  $\beta = 0.1$ ,  $Da = 0.1$ ,  $\kappa = 10$ ,  $Ha = 4$ ,  $\Gamma = 1$ , and  $S = 5$  (color online)

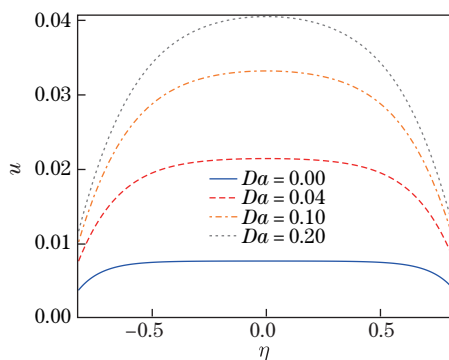


**Fig. 6** Influence of Darcy number on velocity distribution when  $a = 0.05$ ,  $\xi = 0.4$ ,  $\phi = 0.05$ ,  $m = 0.5$ ,  $Ha = 4$ ,  $\beta = 0.1$ ,  $\kappa = 10$ ,  $\Gamma = 1$ , and  $S = 0.1$  (color online)

The variation of the skin friction  $C_f$  with Darcy number  $Da$  for different values of the Hartmann number  $Ha$  is presented in Fig. 7. It is seen that skin friction increases rapidly with increase in Darcy number in the absence of any external magnetic field. This implies that the drag force between the fluid flow and the surface of the microchannel increases with the increase in permeability of the medium, due to which the skin friction is enhanced. However, the external magnetic field can reduce the skin friction significantly. Figure 8 depicts the change in skin friction for a wide range of volume fractions of the nanoparticles and velocity slip. This figure clearly shows that the skin friction reduces appreciably, as the velocity-slip/volume fraction of the nanoparticles rises.

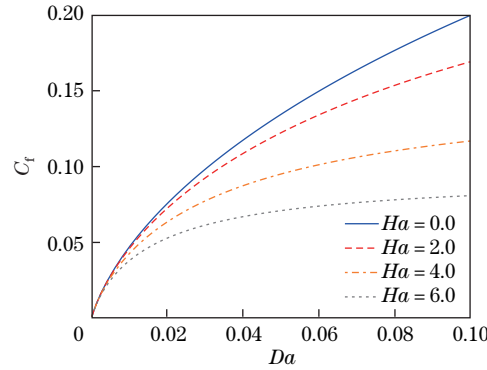


**Fig. 7** Influence of Darcy number and Hartmann number on skin friction ( $C_f$ ) when  $a = 0.05$ ,  $\xi = 0.4$ ,  $\phi = 0.05$ ,  $m = 0.5$ ,  $\beta = 0.1$ ,  $\kappa = 10$ ,  $\Gamma = 1$ ,  $S = 0.1$ , and  $R = -0.5$  (color online)

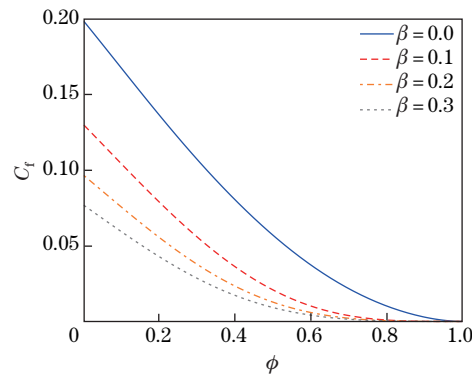
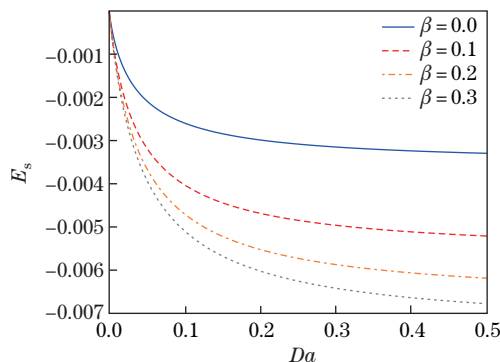


**Fig. 8** Influence of nanoparticle volume fraction and velocity-slip parameter on skin friction ( $C_f$ ) when  $a = 0.05$ ,  $\xi = 0.4$ ,  $Ha = 4$ ,  $m = 0.5$ ,  $S = 0.1$ ,  $Da = 0.1$ ,  $\kappa = 10$ ,  $Ha = 4$ ,  $\Gamma = 1$ , and  $R = -0.5$  (color online)

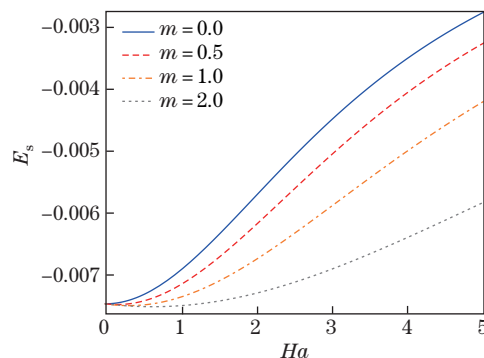
### 3.3 Streaming potential

Figure 9 gives an idea of the variation of streaming potential as the permeability parameter increases. This variation has been examined for several values of the velocity-slip. It may be noticed that for a given Darcy number, the streaming potential is maximum when velocity-slip is absent, and it decreases as the velocity-slip increases. A similar observation is obtained from Fig. 10, which gives the variation of streaming potential with respect to change in magnetic field strength/Hall parameter. It is noticed that the fluid velocity along the capillary-axis is enhanced when the slip velocity at the wall or the permeability increases. These observations imply that owing to the free movement of ionic charges inside the capillary, the streaming

potential is reduced. The relation between the velocity and the streaming potential has been deduced analytically and presented in Eq. (19). In Fig. 4, we have already seen that velocity reduces with increase in magnetic field strength ( $Ha$ ). This may be attributed to the fact that transport of charged ions in the EDL region is considerably affected by magnetic field effect, whereby the streaming potential is enhanced. Similarly, Fig. 5 reveals that an increase in the Hall effect can enhance the fluid velocity. This implies that electrokinetic induction is hindered by the rapid movement of the mobile ions inside the capillary vessel.



**Fig. 9** Influence of Darcy number and velocity-slip parameter on dimensionless streaming potential when  $a = 0.05$ ,  $\xi = 0.4$ ,  $\phi = 0.05$ ,  $m = 0.5$ ,  $Ha = 4$ ,  $\kappa = 10$ ,  $\Gamma = 1$ ,  $S = 5$ , and  $R = -0.5$  (color online)



**Fig. 10** Influence of Hartmann number and Hall parameter on dimensionless streaming potential when  $a = 0.05$ ,  $\xi = 0.4$ ,  $\phi = 0.05$ ,  $\beta = 0.1$ ,  $Da = 0.1$ ,  $\kappa = 10$ ,  $\Gamma = 1$ ,  $S = 5$ , and  $R = -0.5$  (color online)

### 3.4 Heat transfer

Figure 11 illustrates the variation in temperature distribution, when the values of Hall parameter changes. The nature of changes in temperature distribution in the nanofluid is in conformity to the observations made by Zhao et al.<sup>[18–19]</sup>. Figure 11 depicts the impact of Hall current on temperature distribution. This figure shows that the fluid temperature gradually diminishes with the increase in Hall effect. This observation may be attributed to the increase in axial velocity of the nanofluid, which leads to the enhancement of thermal diffusion rate. Owing to the presence of magnetic nanoparticles, the wall shear stress changes and thereby the heat removal capacity of the nanofluid is altered. It may further be observed that in the range of Hall parameter examined here, the temperature profiles have parabolic shapes under the influence of a reasonably strong magnetic field. An opposite trend is observed for the effect of thermal radiation on temperature distribution, where the radiation takes place due



to thermoradiative heat flux (see Fig. 12). It is also revealed that with increase in thermal radiation, there is also gradual enhancement in thermal boundary layer thickness. The plots of Fig. 13 show that the temperature of the nanofluidic mass reduces, as the process of heat generation ( $\varrho > 0$ )/heat absorption ( $\varrho < 0$ ) proceeds, where heat generation/heat absorption is effected by Joule heating. On the basis of the observation of Fig. 13, we may proclaim that Joule heating controls over the maintenance of temperature in the non-uniform capillary under consideration.

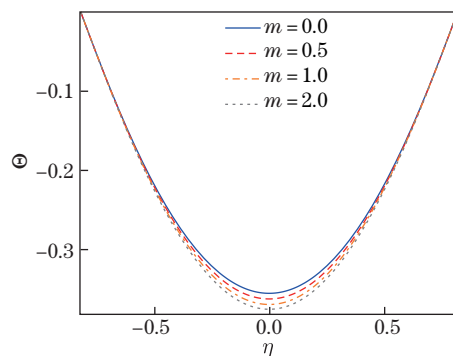


**Fig. 11** Effect of Hall current on distribution of temperature when  $a = 0.05$ ,  $\xi = 0.4$ ,  $\phi = 0.05$ ,  $Da = 0.1$ ,  $\kappa = 10$ ,  $Ha = 6$ ,  $\Gamma = 1$ ,  $R = -0.5$ ,  $\delta = 0$ ,  $S = 5$ ,  $N_r = 1$ ,  $\varrho = 0.2$ , and  $Br = 0.01$  (color online)

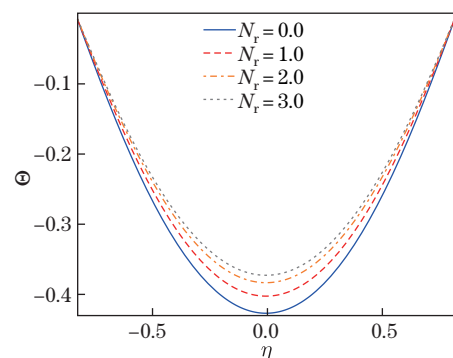


**Fig. 12** Effect of thermal radiation on temperature distribution when  $a = 0.05$ ,  $\xi = 0.4$ ,  $\beta = 0.1$ ,  $Ha = 4$ ,  $Da = 0.1$ ,  $\kappa = 10$ ,  $\Gamma = 1$ ,  $R = -0.5$ ,  $\phi = 0.05$ ,  $\delta = 0.01$ ,  $m = 0.5$ ,  $\varrho = 0.2$ ,  $S = 5$ , and  $Br = 0.01$  (color online)

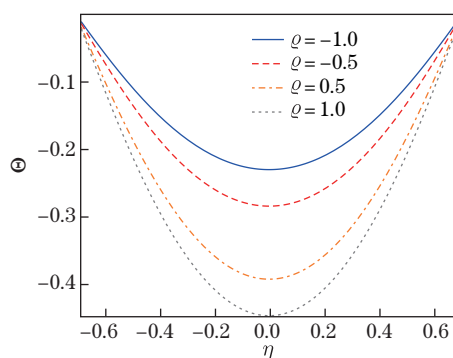


**Fig. 13** Effect of Joule heating on temperature distribution when  $a = 0.05$ ,  $\xi = 0.4$ ,  $\phi = 0.05$ ,  $Da = 0.1$ ,  $\beta = 0.1$ ,  $\kappa = 10$ ,  $Ha = 4$ ,  $\Gamma = 1$ ,  $R = -0.5$ ,  $m = 0.5$ ,  $S = 5$ ,  $N_r = 1$ ,  $\delta = 0.01$ , and  $Br = 0.01$  (color online)

The combined effect of thermal slip and Joule heating has been illustrated in Fig. 14. For heat transfer problems, Nusselt number, i.e., ratio of the convective heat transfer to conductive heat transfer along the direction perpendicular to the mean flow of the fluid bears the potential to provide a better understanding of the physics of the heat transfer process. In view of this, we consider it worthwhile to examine the effects of thermal slip and Joule heating on the change in Nusselt number. We have seen that as thermal slip increases, there occurs a considerable reduction in fluid temperature. This is in concurrence with the observation from Fig. 14, which depicts the variation in Nusselt number ( $Nu$ ) for different Joule heating parameters. This figure shows that Nusselt number decreases as Joule heating parameter increases. Figure 15 shows that as the Hartmann number increases, there is an exponential enhancement in Nusselt number. This figure further shows that due to increasing Hall parameter, heat transfer at the solid-fluid interface of the channel is enhanced. It is important to observe that heat removal is more pronounced in the presence of Hall current under the action of externally applied strong magnetic field. One may further observe that the cooling performance of the system is more efficient in the presence of Hall current.

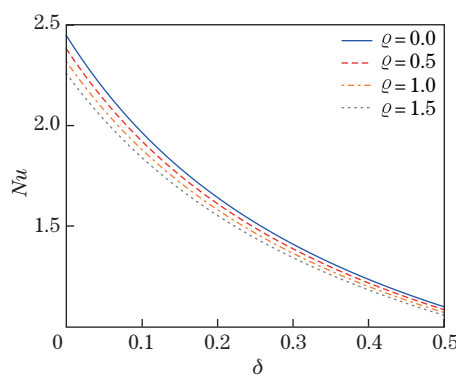


**Fig. 14** Influence of Joule heating and thermal slip on Nusselt number when  $a = 0.05$ ,  $\xi = 0.4$ ,  $\beta = 0.1$ ,  $m = 0.5$ ,  $Ha = 4$ ,  $Da = 0.1$ ,  $\kappa = 10$ ,  $\Gamma = 1$ ,  $R = -0.5$ ,  $\phi = 0.05$ ,  $N_r = 1$ ,  $S = 5$ , and  $Br = 0.01$  (color online)

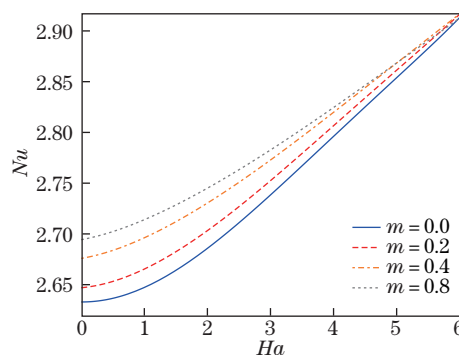


**Fig. 15** Variations of Nusselt number as a function of Hartmann number for different Hall parameters when  $a = 0.05$ ,  $\xi = 0.4$ ,  $Da = 0.1$ ,  $\beta = 0.1$ ,  $\kappa = 10$ ,  $\phi = 0.05$ ,  $S = 5$ ,  $q = 0.2$ ,  $\delta = 0.01$ ,  $N_r = 1$ , and  $Br = 0.01$  (color online)

### 3.5 Entropy generation

Induction of entropy generation during flow/heat transfer of a fluid mass may take place due to thermal diffusion, Joule heating and also by magnetic field/fluid viscosity/medium porosity.

Therefore, it is worthwhile to examine the impact of relevant physical parameters on entropy generation. The extent to which entropy generation ( $S_G$ ) is affected due to the change in Hall parameter has been illustrated in Fig. 16. Since under the purview of the present study, the axial velocity of the nanofluid is enhanced with an increase in Hall current effect, the dispersion of the fluid mass will take place at a faster rate as the Hall effect is more and more pronounced with the increase in the intensity of the magnetic field. Figure 16 further shows that except in the close vicinity of the central line of the microchannel, the entropy decreases with an increase in the Hall parameter. Form Fig. 17, one can have an idea of the change in Bejan number defined by Eq. (38) as Hall parameter increases. It is interesting to note that Bejan number has a vanishing value in the central region of the microchannel. This observation implies that in this region entropy generation is negligibly small, owing to the resultant effect of the electric field, magnetic field, porosity of the medium and the friction of the fluid particles. However, outside the central region the Bejan number is significantly influenced by the Hall current. Figure 17 also indicates that with an increase in Hall effect, thermal irreversibility is drastically reduced in the vicinity of the central line of the microchannel.

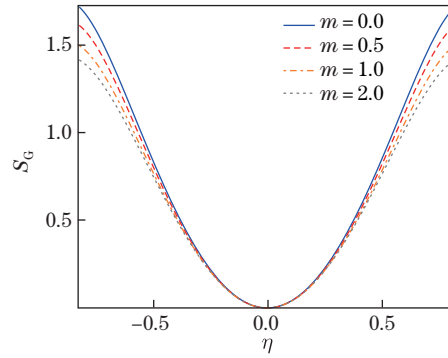


**Fig. 16** Impact of Hall parameter on entropy distribution when  $a = 0.05$ ,  $\xi = 0.5$ ,  $\delta = 0.02$ ,  $\phi = 0.05$ ,  $Ha = 4$ ,  $\beta = 0.1$ ,  $\kappa = 10$ ,  $\Gamma = 1$ ,  $S = 5$ ,  $R = -0.5$ ,  $Da = 0.1$ ,  $N_r = 1$ ,  $\varrho = 0.2$ ,  $Br = 0.01$ ,  $Pe = 1$ , and  $\Re = 1$  (color online)

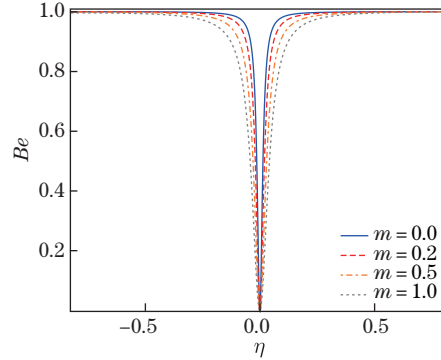


**Fig. 17** Influence of Hall parameter on the Bejan number when  $a = 0.05$ ,  $\xi = 0.4$ ,  $\phi = 0.05$ ,  $Da = 0.1$ ,  $\kappa = 10$ ,  $Ha = 4$ ,  $\Gamma = 1$ ,  $R = -0.5$ ,  $S = 5$ ,  $N_r = 1$ ,  $\delta = 0.1$ ,  $\varrho = 0.1$ ,  $Pe = 1$ ,  $Br = 0.01$ , and  $\Re = 1$  (color online)

#### 4 Concluding remarks

The study deals with a theoretical investigation of fully developed nanofluid flow on a porous microchannel having wavy geometry, when the flow is thermally induced and is under the combined influence of an electric field, a magnetic field and a pressure gradient applied externally.

Impact of Hall current and streaming potential on entropy generation and transfer of heat in case of electrokinetically induced flow of a nanofluid has been of prime interest in the study. While the theoretical study has been performed for a nanofluid in general, the computational work has been carried out for electrokinetic flow in the microcirculatory system, when representative base fluid is mixed with nanoparticles of  $\text{Fe}_3\text{O}_4$ . The observations derived from the study lead us to conclude the following.

(i) Axial velocity of fluid in an artery can be reduced by increasing the strength of the applied magnetic field. However, due to the presence of Hall current, axial velocity is enhanced. The study indicates that during MRI, due to interaction between magnetic field and induced current, a significant reduction in flow rate takes place, if the magnetic field is sufficiently strong.

(ii) Flow in the porous microchannel increases with an increase in Darcy number. Quantitatively, the velocity along the central line is 4 times more in the case of a porous microchannel ( $Da = 0.2$ ) than that when it is non-porous ( $Da \rightarrow \infty$ ) at  $\xi = 0.4$ .

(iii) Streaming potential reduces, when there is a rise in the porosity of the channel/velocity-slip/Hall current.

(iv) Nanofluidic temperature is enhanced with the increase in volume fraction of nanoparticle in nanofluid/thermal radiation, but it is reduced with the increase in Hall current/Joule heating.

(v) Hall effect enhances the cooling performance of the system. Due to Hall current, there is a rise in the Nusselt number by nearly 3%, when  $m$  increases from 0 to 1.

(vi) Nusselt number reduces with increase in Joule heating/thermal slip.

(vii) Quantum of entropy generation in the neighborhood of the channel wall is more than that in the central region.

(viii) Thermal irreversibility is lowered due to increase in the Hall effect.

The study bears the potential of important applications in magnetic resonance angiography (MRA), which encounters the combined effect of Hall current and a sufficiently strong magnetic field. Clinicians engaged in the treatment of cancer will find the study useful in the application of chemotherapy, where nanoparticles are suitably mixed with blood in order to inhibit the growth of blood cells. Since ferromagnetic nanoparticles are known to be very good carriers of drug, observations of the study are useful for drug delivery.

**Acknowledgements** The authors wish to express their deep sense of gratitude to the esteemed editor and all the reviewers for their useful suggestions for the improvement of the original manuscript. They are also thankful to the Science and Engineering Research Board (SERB), Department of Science and Technology, Government of India, New Delhi for the financial support through Grant No. CRG/2018/000153.

## References

- [1] OHNO, K., TACHIKAWA, K., and MANZ, A. Microfluidics: applications for analytical purposes in chemistry and biochemistry. *Electrophoresis*, **29**(22), 4443–4453 (2008)
- [2] SHOJI, S., NAKAGAWA, S., and ESASHI, M. Micropump and sample injector for integrated chemical analysis systems. *Sensors and Actuators A*, **21**, 189–192 (1990)
- [3] BECKER, H. and GARTNER, C. Polymer microfabrication methods for microfluidic analytical applications. *Electrophoresis*, **21**(1), 12–26 (2000)
- [4] CHAKRABORTY, R., DEY, R., and CHAKRABORTY, S. Thermal characteristics of electro-magnetohydrodynamic flows in narrow channels with viscous dissipation and Joule heating under constant wall heat flux. *International Journal of Heat and Mass Transfer*, **67**, 1151–1162 (2013)
- [5] SI, D. Q. and JIAN, Y. J. Electromagnetohydrodynamic (EMHD) micropump of Jeffrey fluids through two parallel microchannels with corrugated walls. *Journal of Physics D: Applied Physics*, **48**, 085501 (2015)

- [6] BUREN, M., JIAN, Y. J., and CHANG, L. Electromagnetohydrodynamic flow through a microparallel channel with corrugated walls. *Journal of Physics D: Applied Physics*, **47**, 425501 (2014)
- [7] ARIFIN, D. R., YEO, L. Y., and FRIEND, J. R. Microfluidic blood plasma separation via bulk electrohydrodynamic flows. *Biomicrofluidics*, **1**(1), 014103 (2007)
- [8] ABHIMANYU, P., KAUSHIK, P., MONDAL, P. K., and CHAKRABORTY, S. Transiences in rotational electro-hydrodynamics microflows of a viscoelastic fluid under electrical double layer phenomena. *Journal of Non-Newtonian Fluid Mechanics*, **231**, 56–67 (2016)
- [9] CHANDRA, S. and MISRA, J. C. Influence of Hall current and microrotation on the boundary layer flow of an electrically conducting fluid: application to hemodynamics. *Journal of Molecular Liquids*, **224**, 818–824 (2016)
- [10] MISRA, J. C., CHANDRA, S., and HERWIG, H. Flow of a micropolar fluid in a micro-channel under the action of an alternating electric field: estimates of flow in bio-fluidic devices. *Journal of Hydrodynamics*, **27**, 350–358 (2015)
- [11] MISRA, J. C. and SINHA, A. Electro-osmotic flow and heat transfer of a non-Newtonian fluid in a hydrophobic microchannel with Navier slip. *Journal of Hydrodynamics*, **27**, 647–657 (2015)
- [12] MISRA, J. C., CHANDRA, S., SHIT, G. C., and KUNDU, P. K. Electroosmotic oscillatory flow of micropolar fluid in microchannels: application to dynamics of blood flow in microfluidic devices. *Applied Mathematics and Mechanics (English Edition)*, **35**(6), 749–766 (2014) <https://doi.org/10.1007/s10483-014-1827-6>
- [13] MISRA, J. C. and CHANDRA, S. Electro-osmotically actuated oscillatory flow of a physiological fluid on a porous microchannel subject to an external AC electric field having dissimilar frequencies. *Central European Journal of Physics*, **12**(4), 274–285 (2014)
- [14] MISRA, J. C. and CHANDRA, S. Electro-osmotic flow of a second-grade fluid in a porous microchannel subject to an AC electric field. *Journal of Hydrodynamics*, **25**, 309–316 (2013)
- [15] MISRA, J. C., SHIT, G. C., CHANDRA, S., and KUNDU, P. K. Electro-osmotic flow of a viscoelastic fluid in a channel: applications to physiological fluid mechanics. *Applied Mathematics and Computation*, **217**, 7932–7939 (2011)
- [16] JIAN, Y. J. Transient MHD heat transfer and entropy generation in a microparallel channel combined with pressure and electroosmotic effects. *International Journal of Heat and Mass Transfer*, **89**, 193–205 (2015)
- [17] SINHA, A. and SHIT, G. C. Electromagnetohydrodynamic flow of blood and heat transfer in a capillary with thermal radiation. *Journal of Magnetism and Magnetic Materials*, **378**, 143–151 (2015)
- [18] ZHAO, G., JIAN, Y., and LI, F. Streaming potential and heat transfer of nanofluids in microchannels in the presence of magnetic field. *Journal of Magnetism and Magnetic Materials*, **407**, 75–82 (2016)
- [19] ZHAO, G., JIAN, Y., and LI, F. Streaming potential and heat transfer of nanofluids in parallel plate microchannels. *Colloids and Surfaces A: Physicochemical and Engineering Aspects*, **498**, 239–247 (2016)
- [20] MISRA, J. C. and ADHIKARY, S. D. Flow of a Bingham fluid in a porous bed under the action of a magnetic field: application to magneto-hemorheology. *Engineering Science and Technology, an International Journal*, **20**, 973–981 (2017)
- [21] SCHENCK, J. F. Safety of strong, static magnetic fields. *Journal of Magnetic Resonance Imaging*, **12**(1), 2–19 (2000)
- [22] COWLING, T. G. *Magnetohydrodynamics*, InterScience, New York (1975)
- [23] BEJAN, A. Second law analysis in heat transfer. *Energy*, **5**, 720–732 (1980)
- [24] SINGH, P. K., ANOOP, K. B., SUNDARARAJAN, T., and DAS, S. K. Entropy generation due to flow and heat transfer in nanofluids. *International Journal of Heat and Mass Transfer*, **53**, 4757–4767 (2010)
- [25] MAHMOUDI, A. H., POP, I., SHAHI, M., and TALEBI, F. MHD natural convection and entropy generation in a trapezoidal enclosure using Cu-water nanofluid. *Computer and Fluids*, **72**, 46–62 (2013)

- [26] MATIN, M. H. and KHAN, W. A. Entropy generation analysis of heat and mass transfer in mixed electrokinetically and pressure driven flow through a slit microchannel. *Energy*, **56**, 207–217 (2013)
- [27] ABDALLA, S., AL-AMEER, S. S., and AL-MAGAISHI, S. H. Electrical properties with relaxation through human blood. *Biomicrofluidics*, **4**, 034101 (2010)
- [28] SIMA, W., SHI, J., YANG, Q., HUANG, S., and CAO, X. Effects of conductivity and permittivity of nanoparticle on transformer oil insulation performance: experiment and theory. *IEEE Transactions on Dielectrics and Electrical Insulation*, **22**(1), 380–390 (2015)
- [29] XUAN, Y. and LI, Q. Investigation on convective heat transfer and flow features of nanofluids. *ASME Journal of Heat Transfer*, **125**, 151–155 (2003)
- [30] YU, W. and CHIO, S. U. S. The role of interfacial layers in the enhanced thermal conductivity of nanofluids: a renovated Maxwell model. *Journal of Nanoparticle Research*, **5**, 167–171 (2003)
- [31] SUTTON, G. W. and SHERMAN, A. *Engineering Magnetohydrodynamics*, Mc Graw-Hill, New York (1965)
- [32] MOHAMED, R. A. and ABO-DAHAB, S. M. Influence of chemical reaction and thermal radiation on the heat and mass transfer in MHD micropolar flow over a vertical moving porous plate in a porous medium with heat generation. *International Journal of Thermal Sciences*, **48**, 1800–1813 (2009)
- [33] HUNTER, R. J. *Zeta Potential in Colloid Science*, Academic Press, London/New York (1981)
- [34] MASLIYAH, J. H. and BHATTACHARJEE, S. *Electrokinetic and Colloid Transport Phenomena*, Wiley, Hoboken/New Jersey (2006)
- [35] CHAKRABORTY, S. and ROY, S. Thermally developing electroosmotic transport of nanofluids in microchannels. *Microfluidics and Nanofluidics*, **4**, 501–511 (2008)
- [36] QIAN, S. and BAU, H. H. Magneto-hydrodynamic based microfluidics. *Mechanics Research Communications*, **36**, 10–21 (2009)
- [37] THOMPSON, P. A. and TROIAN, S. M. A general boundary condition for liquid flow at solid surface. *nature*, **389**, 360–362 (1997)
- [38] MISRA, J. C., MALLICK, B., SINHA, A., and ROYCHOWDHURY, A. Impact of Cattaneo-Christov heat flux on electroosmotic transport of third-order fluids in a magnetic environment. *The European Physical Journal Plus*, **133**(5), 195 (2018)
- [39] BEJAN, A. A study of entropy generation in fundamental convective heat transfer. *Journal of Heat Transfer*, **101**(1), 718–725 (1979)
- [40] HIGASHI, T., YAMAGISHI, A., TAKEUCHI, N., KAWAGUCHI, N., SAGAWA, S., ONISHI, S., and DATE, M. Orientation of erythrocytes in a strong static magnetic field. *Blood*, **82**, 1328–1334 (1993)